applied sciences

MDPI

Article

Effect of Three-Dimensional (3D) Scanning Factors on Minimizing the Scanning Errors Using a White LED Light 3D Scanner

Syed Farhan Raza [1], Muhammad Amjad [2,*], Kashif Ishfaq [1], Shafiq Ahmad [3] and Mali Abdollahian [4]

[1] Department of Industrial and Manufacturing Engineering, University of Engineering and Technology, Lahore 54890, Pakistan
[2] Department of Mechanical, Mechatronics and Manufacturing Engineering, New Campus, University of Engineering and Technology, Lahore 54890, Pakistan
[3] Industrial Engineering Department, College of Engineering, King Saud University, P.O. Box 800, Riyadh 11421, Saudi Arabia
[4] School of Science, College of Sciences, Technology, Engineering, Mathematics, RMIT University, P.O. Box 2476, Melbourne, VIC 3001, Australia
* Correspondence: amjad9002@uet.edu.pk

Highlights:

What are the main findings?

- Of the main effects, MW and simplification (70%) were found to be optimal levels of watertight and simplification in almost all the scanning modes, regardless of sample geometry. Moreover, two sample geometries were scanned three dimensionally and are referred to as simple and complex samples in this research;
- The scanning errors were found to be lower for the complex sample, i.e., up to 0.1%, when compared to errors for the simple sample. The reduction in error up to such an extent was never reported before;

What are the implications of main findings?

- Three-dimensional scanning research implies that the scanning of complex product components is preferred to the scanning of simple components, which may be easily modelled geometrically.
- Mode A of 3D scanning for complex sample was evaluated to be the optimal among all other modes of 3D scanning.

Abstract: The largest problem with scanning real objects involves bearing the huge costs of scanning and the low quality of point cloud data for a scanned object, thereby increasing the cost and lead time. Therefore, a need exists to improve the quality of scanning to save time, costs, and computational resources. In this research, the levels of optimal factors associated with a three-dimensional (3D) scanner were investigated, improving the quality of 3D scanning data. Optimizing the 3D scanner factors could help us acquire errorless digital scanned data that accurately resemble a 3D physical object and which may be further used in various engineering applications, e.g., additive manufacturing and non-engineering applications. For this study, four modes of 3D scanning (A, B, C, and D) were utilized with five crucial 3D scanning factors namely texture, watertightness, simplification, and alternate deployments of smoothness and sharpness. This research was divided into two stages. The former stage involved the 3D scanning of two samples with simple and complex geometrical intricacies and the later stage involved checking the scanned objects for any dimensional errors. A coordinate measuring machine (CMM) was used to measure the dimensional details of the real objects. For virtual metering, Solidworks was utilized. With reference to the limited literature in the current context, 3D scanning errors were highly reduced for the first time up to 0.1% for the complex sample when compared to the errors found for the simple sample.

Citation: Raza, S.F.; Amjad, M.; Ishfaq, K.; Ahmad, S.; Abdollahian, M. Effect of Three-Dimensional (3D) Scanning Factors on Minimizing the Scanning Errors Using a White LED Light 3D Scanner. *Appl. Sci.* **2023**, *13*, 3303. https://doi.org/10.3390/app13053303

Academic Editor: César M. A. Vasques

Received: 30 January 2023
Revised: 1 March 2023
Accepted: 2 March 2023
Published: 5 March 2023

Keywords: reverse engineering; three-dimensional (3D) scanning; watertight; simplification; percent contribution (PCR); severity index (SI)

1. Introduction

Three-dimensional scanning has various applications in reverse engineering (RE), medicine, cultural artifacts, rapid prototyping, quality inspection, industry 4.0, industrial design, textiles, dentistry, prosthetics, and implants. Product development cycles take a considerable amount of cost and time, and 3D scanning can help product developers reduce the costs and lead time involved in terms of meeting the market demand, customer needs, requirements to change the design, redesigning, reengineering, etc. Therefore, the increased digitization of the product leads to greater possibilities of bringing about real change in the product design without wasting time and money. The images captured from a 3D scanner are analyzed using high-performance computers (HPC) with the help of compatible software. The software utilized for image analysis is either built-in for the 3D scanner or others, which include SolidWorks, Geomagic Design X, and the Geomagic plugin for SolidWorks, etc. [1].

Digitizing the manufacturing sector is a topic of extensive debate these days, resulting in huge time savings, significant economic throughput, precision and accuracy, and an enhanced automation level. Three-dimensional scanning plays an important role in the digitization of the manufacturing world. It has also strong applications in the reverse engineering (RE), which is helpful in those situations where a physical model of the engineering component is available without its virtual counterpart. [2,3]. The purpose of 3D scanning is to transfer the real, physical object from a real-world environment into a digital object in a virtual environment. A 3D scanner gathers critical object information and a crucial level of detail regarding size and shape for further processing, such as 3D/4D printing, with the fact that additive manufacturing is a potential candidate for Industry 4.0 [4]. I. G. Perez and A. F. Aznar [5] applied a reverse engineering approach using a non-contact laser 3D scanner on geometric modelling to improve spiral bevel gears. Although the authors put effort into reverse engineering crucial milling gears, they accepted that the error controls did not remain tight during their work despite their due considerations toward errors.

As far as 3D scanning methodologies are concerned; contact, non-contact, and hybrid methods are three well-known methods of 3D scanning. When compared to the stylus/probe used to make contact with the surfaces in the contact methods, the non-contact method does not use any contacting tool such as stylus or probe to capture the dimensions of mechanical components. In fact, non-contact methods utilize various media including light, lasers, sound, magnetic fields, and X-rays to digitize the mechanical components with greater time savings. A 3D scanner using sensors, blue light, light-emitting diodes (LEDs), and cameras is a non-contact type of 3D scanner. The hybrid method of 3D scanning involves using both contact and non-contact methods together. Hybrid methods are used for scenarios in which the disadvantages of contact and non-contact methods must be fixed. For instance, non-contact methods consume lot of time to achieve a complete scan; on the other hand, inaccuracies are always encountered when using contact methods [2].

Three-dimensional scanning plays a vital role in engineering and in the medical sectors. In medical use, 3D scanning helps practitioners find the causes of various illnesses. Medical 3D scanning technologies include X-rays, computed topology (CT), ultrasounds, and magnetic resonance imaging (MRI). CT scans, X-rays, and MRIs fall into the category of non-contact methods of 3D scanning, whereas the ultrasound is a contact method of 3D Scanning. Three-dimensional scanning for medical applications involves producing medical implants that are nearly like the originals with specific standards. Three-dimensional scanning is very helpful to practitioners for accurately measuring the shape of a patient's bodily components with the aim of acquiring them physically. Non-contact-type 3D scanning is

fully accomplished by multiple scan passes of a physical object, which is either stationary or rotatory to explore all surfaces during scanning. The scanned surfaces are then merged to obtain a digital model using the triangulation method technique [6]. N. Anwer and L. Mathieu [7] studied reverse engineering as a tool for acquiring the digital shape. They found that there are three main sub-processes of the reverse engineering process, which include digitization, shape reconstruction, and computer-aided design (CAD) modeling. Although the authors attempted to achieve a framework of reverse engineering, the time required to attain a digital product was higher due to various lengthy processes, such as shape reconstruction. Moreover, shape reconstruction is automatically achieved these days using the latest 3D scanners. In another research study conducted by Qie et al. [8], the authors devised a relationship between the general functions for merging the local and global features of parts and assemblies by employing certain principles, machine learning, and a similarity search as a part of the shape reconstruction process. Though the authors endeavored to determine the finest method of reverse engineering, the research work again appeared to be time-consuming and basically lacked a reduction in the lead time.

F. Bauer et al. [9] put their effort towards repairing or replacing turbine blades, utilizing the selective laser melting process when implementing the reverse-engineering process. They used optical scanning and CT scanning for the turbine blades as the blueprints for these blades were not available. The resulting turbine blade replicas were expected to greatly help the research and development (R&D) teams reduce the detrimental downtimes. Y. Yang et al. [10] developed an algorithm for subtle feature extraction when reverse engineering complex and irregular surfaces. The obtained results were quite helpful towards high precision machining as a guide. The feature extraction algorithm involved using point cloud data with the capability to accurately reach the correct details of a feature. The developed algorithm was also found to be more accurate when it was compared to other algorithms available from past studies. Yanamandra et al. [11] used imaging technology for the additive manufacturing of composite materials. A dimensional accuracy of the reverse engineering model of 0.33% was achieved by the authors. Although the authors worked on the dimensional accuracy of the scanned model, the dimensional errors were found to be higher and need to be reduced with better 3D scanning methodologies.

Che et al. [12] devised a unique way of determining milling tool performance based on reverse engineering. Though the authors employed the latest tools, including 3D scanning, finite element analysis (FEA), and an empirical validation of FEA, they did not consider the quality of 3D scanning able to ensure precision in reverse engineering. P. Wang et al. [13] employed a unique technical route to design and manufacture a helmet using reverse engineering and 3D/4D printing technologies. Three-dimensional scanning was used as a crucial step in reverse engineering without the geometrical definitions of a helmet. Liu et al. [14] performed a parametric optimization of the spot-welding process using reverse engineering principles and direct FEA. Stamping parts with back-side panels were investigated to evaluate the deformations.

T. Segreto et al. [15] compared the scanning quality of two 3D scanning or reverse-engineering systems, namely, a portable measuring arm (PMA) with a laser scanner and digital close-range photogrammetry (DCRP), for both the virtual construction of and real repair work on cultural heritage artifacts. It was found that the PMA laser system was more precise and accurate; however, the DCRP system was less costly and time consuming. T. Segreto et al. [16] again combined laser scanning and a non-contact ultrasonic tool to detect the external geometry and internal material structure of carbon-fiber-reinforced polymers (CFRPs). It was a unique way of digitizing the geometry and acquiring the material structure; however, they could not properly address the dimensional error that arose during 3D scanning. S. S. H. Al-Maeeni and B. Engel [17] integrated reverse engineering, non-destructive inspections, and FEA to redefine a shaft when its blueprints were unavailable.

Irzman' ska and Okrasa [18] applied 3D scanning methodology to improve the ergonomic aspect of footwear. Three-dimensional scanning has already proven itself to be very effective at digitizing objects. The footwear dimensions were accurately measured with sufficient precision using 3D scanning.

Haleem and Javaid [19] employed 3D scanning technology in the medical field to digitize bodily information. The research on 3D scanning in the medical field is perpetually being enhanced. Three-dimensional scanning is also being utilized in prosthetics and implantation. It also effectively scans the exterior body parts of patients in 3D form. Thanks to 3D scanning technology, medical practitioners may efficiently and effectively expedite the treatment process for dangerous diseases. The same authors also identified the eight steps methodology [20], which initiates with the diagnosis of an issue in a patient and ends with a proper surgery. In addition, Maloney [21] explored the potential of 3D scanning technology to deeply examine defect areas in stone. Three-dimensional scanning can also be employed for the effective identification of flake mass. Andrews et al. [22] identified 3D scanning technology as a non-contact technology that can likely enhance the performance of medical staff and the satisfaction of patients.

E. Piperi et al. [23] worked on the reflection issue in 3D scanning for 3D objects used in the automotive industry. Although the authors fixed the issue by spraying the object surfaces with a particle coating, scanned data with proper surface details and precise and accurate dimensional analyses were not addressed appropriately. I. Bodi et al. [24] utilized CAD/CAM systems in the footwear industry to save time and money without compromising the quality and production of shoe manufacturing. The authors applied the simulation features of CAD/CAM systems, which are based on 3D geometric modelling, to possible errors prior to the production of shoes. Paper et al. [25] performed a detailed 3D scanning study which deliberately focused on dimensional errors of the human body. Human body scanning was considered for helping textile industries with respect to introducing rapid alterations in body size to their production efforts. Different parts of the body remained under consideration for the investigation of any difference between their manual and digital dimensions. In their another study, Galantucci et al. [26] used a 3D slit laser scanner for reverse engineering (RE). Although laser scanners are comparatively slower when compared with structured light scanners, the precision and accuracy of laser scanners are usually considered higher. This was, again, not verified in this study. E. Piperi et al. [27] extended their study of 3D scanning to develop low-cost scanning techniques other than structured light and laser scanners. It could have been a brilliant idea to compare the 3D scanning results from both structured light and laser scanners. A. Vazzana et al. [28] explained the steps that are essential in the accurate digitization of archaeological teeth for their successful restoration. These steps mainly included computed micro tomography, the creation of a 3D digital model using reverse engineering, rapid prototyping, and painting where appropriate.

Lazarevic' et al. [29] described another role of 3D scanning which could revolutionize the whole digital manufacturing world, applying scanning techniques to the inspection of manufactured parts in material cutting processes. Dimensional measurements were precisely acquired via 3D scanning and compared to those obtained from a CMM. Conclusively, 3D scanning was found to deliver a better inspection of the manufactured parts, resulting in a substantial reduction in lead time.

Feng et al. [30] explained that preliminary geometric errors are frequently obtained during 3D scanning. Point cloud scanning data usually result from the 3D scanning of physical objects. A self-balancing process can help 3D scanners reduce these geometric deviations; however, this self-balancing process is hard to understand and implement. Therefore, a reasonable gap exists in motivating us to find a convenient way of reducing scanning errors.

Javaid et al. [31] highlighted another application of 3D scanning in dentistry. Dental implants can easily be made using 3D scanning techniques. Moreover, 3D scanning may likely be employed for the innovative creation of dentures, braces, veneers, and aligners. Dentistry teaching–learning methodology may also be improved using scanners.

As can be seen from the previous studies, there is not even one single study on the systematic methodology of three dimensionally digitizing physical components that greatly emphasizes reducing 3D scanning errors. Error-free digital models can confidently be used to accurately and precisely implement the reverse-engineering theory in various engineering disciplines, e.g., additive manufacturing and non-engineering fields. After establishing a 3D scanning methodology, it must be optimized for the 3D scanning factors employed in the established methodology by using the appropriate statistical tools, resulting in a considerable reduction in 3D scanning errors. Past studies merely focused on the construction of the digital shapes of scanned objects without giving due attention to the right framework of 3D scanning. Therefore, a reasonable gap is present, leading us to investigate the acquisition of an optimal framework for 3D scanning, which will ultimately result in error-free digitally scanned objects. Therefore, this study is an effort to fill this gap, presenting the dimensional analyses of various physical objects of varying geometrical intricacies. The expected outcomes of this study include the substantial mitigation of 3D scanning errors. This method of reducing scanning errors may help experts to select an appropriate scanning methodology in diverse fields such as engineering, medicine, textiles, ergonomics, industry 4.0, cultural artifacts, additive manufacturing, and rapid prototyping. Both CMM and Solidworks were used for the first time to conduct a powerful dimensional comparison physically and virtually, respectively, for different geometries with an objective function of reducing 3D scanning errors.

2. Materials and Methods

A 3D scanner based on white LED light, known as the EinScan 3D Scanner, was used in this research. This 3D scanner consists mainly of three components: a turntable, scanner stand, and scanner head, as shown in Figure S1 of the Supplementary File. White LED light is thrown from the scanner head onto the physical object that is placed on the turntable. The round turntable also determines the maximum and minimum size limits of the 3D physical objects to be scanned. The maximum size limit is $200 \times 200 \times 200$ mm^3. Physical objects with a size of less than $30 \times 30 \times 30$ mm^3 are not recommended for the EinScan 3D Scanner. Almost any three-dimensional, intricate physical object (which is nonglossy, not shiny, or non-reflective) may be scanned whose geometric dimensions do not exceed the prescribed size limits.

To keep the experimental methodology simple, a simple box object (i.e., sample one, or S1) and a complex geometrical object (i.e., sample two, or S2) were investigated in this work, as shown in Figures 1 and 2. Engineering drawings with dimensions and tolerances for Figures 1 and 2 are presented as per the guidelines described by the American Society of Mechanical Engineers' standard, known as ASME Y14.5- 2009.

After the object was bombarded with light patterns, the resulting light patterns were then received by the video camera to finally digitize the physical object, termed the "3D scanned object". Before the object was scanned and further used for additive manufacturing, the quality of the 3D scanning was largely affected by the 3D scanning factors and their levels, which were set using EinScan Software. A full factorial design of the experiment (DOE) was conducted in this research, using five 3D scanning factors for samples S1 and S2. These factors can be divided into two categories based on the 3D scanner's operation, i.e., factors set before (pre-scanning factors) and after (post-scanning factors) 3D scanning.

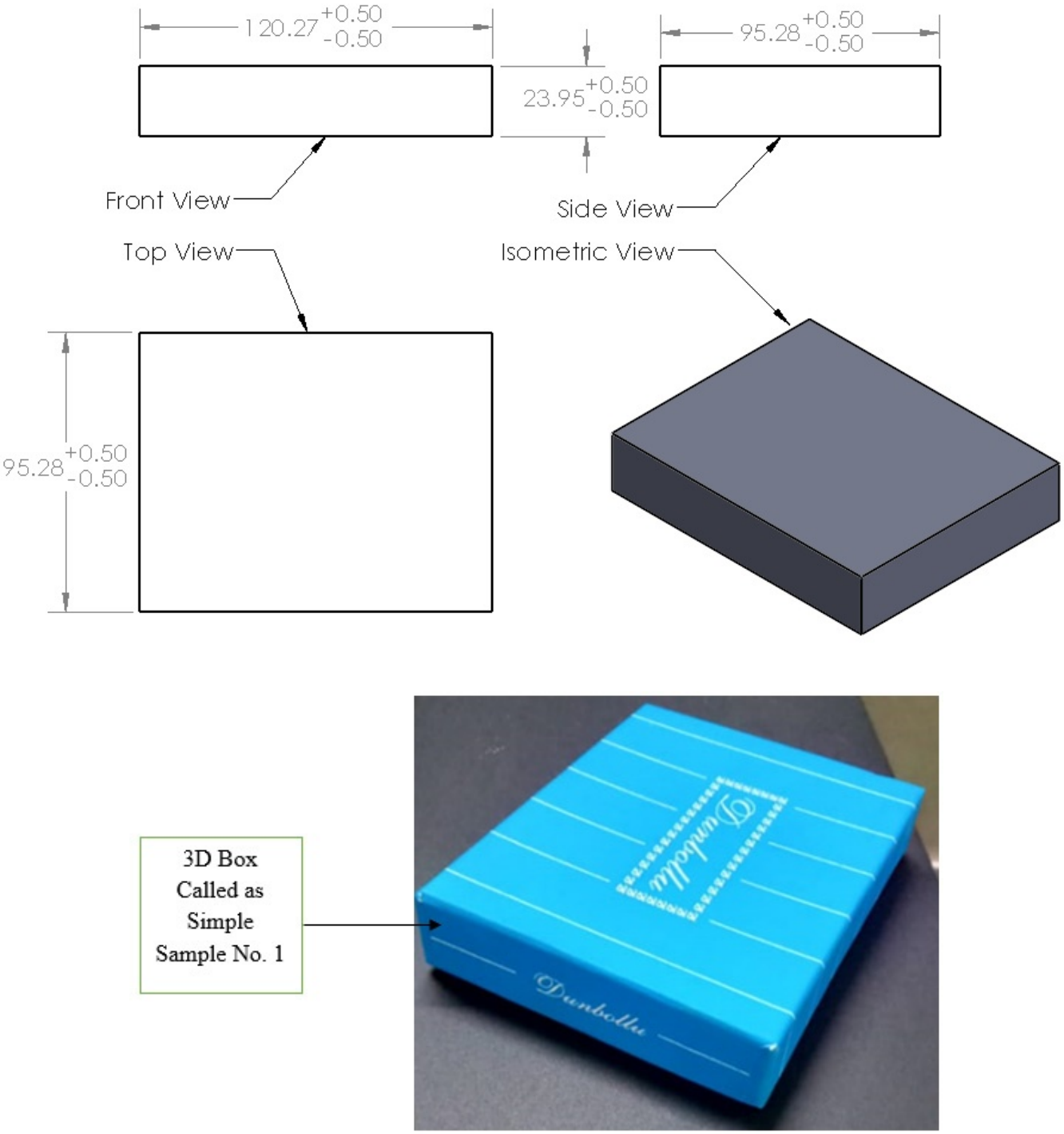

Figure 1. Geometric dimensions of Sample 1 (S1) (mm).

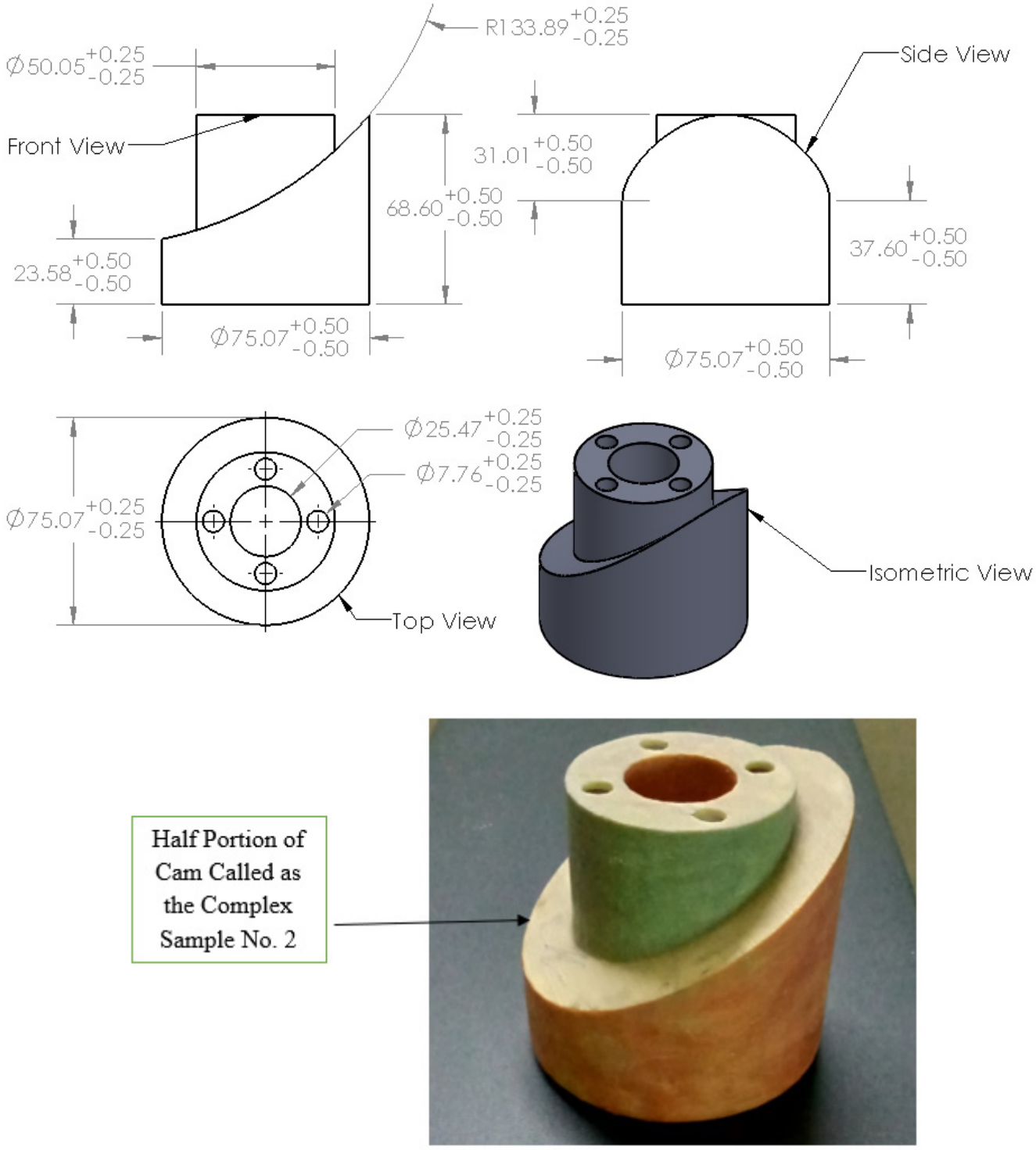

Figure 2. Geometric dimensions of complex object (S2) (mm).

2.1. Factor Settings before 3D Scanning (Pre-Scanning Factors)

The factors set before scanning involved selecting the texture or non-texture option, which depends on the aesthetics of physical object. When the object is colorful, texture scanning becomes essential for acquiring aesthetic details in addition to the geometric information; otherwise, the non-texture scan option is selected. Therefore, there are two possible levels of texture as a factor of 3D scanning: they are simply texture and non-texture. Both the simple and complex samples were scanned with the texture scan option, as shown

in Figure 3. Additionally, colorless digital objects can be obtained, as is shown in Figure 4, with the non-texture scan option even if the samples were originally colorful.

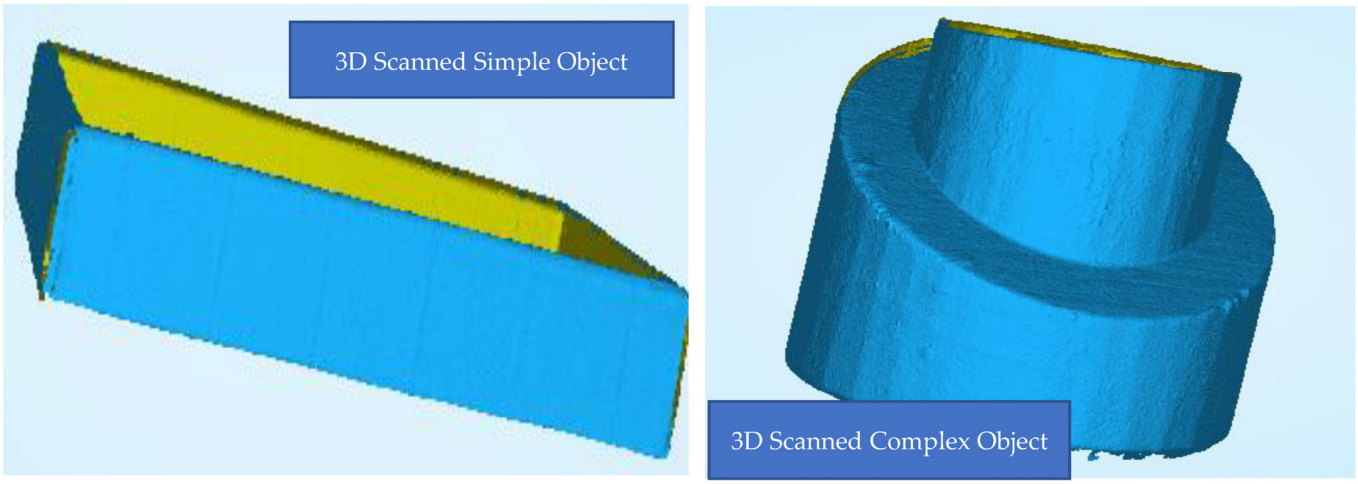

Figure 3. Three-dimensional scanned sample geometries with texture scan option.

Figure 4. Colorless scanned object from non-texture scan.

2.2. Factor Settings after 3D Scanning (Post-Scanning Factors)

The four factors set after scanning consist of watertightness, simplification, smoothness, and sharpness. Post-scanning factors of 3D scanning are necessarily employed as scanned data are obtained in terms of mesh or point cloud, which strongly needs to be post-processed to reduce data noise and defects with data optimization. When completing the 3D scanning of an object, two immediate options are usually presented in a pop-up window in the EinScan software, i.e., watertight and un-watertight. Watertight and un-watertight are two types of 3D geometric models that imply whether models are closed or unclosed, respectively. As 3D scanned geometric models are virtually complex, watertight models are deemed ready for 3D printing. On the other hand, un-watertight models are not closed and may have open surface patches/holes within the 3D scanned model. Moreover, un-watertight models are not ready for 3D printing and point cloud data need to be further processed (WaterTight_UnWaterTight_WebBlog.pdf, 2022). Watertightness has three levels,

i.e., high detail watertight (HW), medium detail watertight (MW), and low detail watertight (LW). The HW level of watertightness is selected when a fine-texture geometric model is desired, and a smooth-textured geometric model results from MW and LW. Together, the watertight factor has four levels in this study. Namely, HW, MW, and LW represent levels of watertightness, and the fourth level is un-watertight (UW). In addition, four levels of watertightness were set when the texture mode of 3D scanning was used. When the non-texture mode of 3D scanning was employed, only two levels were available: MW and UW.

Another post-processing factor is simplification. Simplification simplifies the point cloud data by filling holes using polygon numbers, sizes, and the surface of the data. Its default value is 100%. In this research, three levels of simplification were used: 50%, 60%, and 70%. Therefore, the simplification levels were kept lower than 100% as high percentages of simplification may reduce the actual size of holes which a physical object possess in the details of its features.

Smoothness is another post-processing factor. Smoothness imparts a great effect on the scanned data in terms of removing noise from the data. Finally, sharpness (a post-processing factor) provides better clarity of the scanned data and improves the visual appearance of the scanned data up to an optimum scanning quality.

Based on the settings of the levels of the factors in Table 1, four modes of 3D scanning (A, B, C, and D) were defined for devising novel frameworks of 3D scanning comprising pre- and post-processing factors. These 3D scanning modes were equally applied to S1 and S2, as shown in Table 2.

Table 1. Three-dimensional scanner factor levels.

Factors	Levels
Texture with Sharpness/Smoothness	
Watertightness	4 (LW, MW, HW, and Un-watertight)
Simplification	3 (50%, 60%, and 70%)
Non-Texture with Sharpness/Smoothness	
Watertightness	2 (MW and UW)
Simplification	3 (50%, 60%, and 70%)

Table 2. Modes of 3D scanning.

Modes	3D Scanning Factors *					
	Watertightness	**Simplification**	**Texture**	**Non-Texture**	**Smoothness**	**Sharpness**
A.	✓	✓	✓	✗	✓	✗
B.	✓	✓	✓	✗	✗	✓
C.	✓	✓	✗	✓	✓	✗
D.	✓	✓	✗	✓	✗	✓

* Check (✓) sign implies corresponding 3D scanning factor is kept ON. Cross (✗) sign implies that a particular 3D scanning factor is OFF.

Therefore, a total of twenty-four experiments were conducted for texture scans with sharpness/smoothness and twelve experiments were performed for non-texture scans with sharpness/smoothness. Therefore, the final experiments totaled thirty-six for each sample geometry in this research. Thus, a set of seventy-two experiments were finally conducted for both samples based on a full factorial DOE.

For physical metrology, a coordinate measuring machine (CMM) was used to measure the dimensional input parameters of the samples. The 3D scanned samples, as illustrated in Figure 3, were imported to SolidWorks in stl. format to measure the dimensional output

parameters in a virtual environment, termed the "scanned results." Finally, dimensional errors were measured using scanned and CMM results. The dimensional error was calculated using Equation (1). Scanning errors were found for various features of the geometric model such as the length, width, height, diameter, etc. For overall volumetric errors, Equation (2) was used. In Equations (1) and (2), the term "scanned" implies the virtually measured outcomes, and the term "original" indicates the real measurements from the CMM.

$$\text{DE (\%)} = |(\text{SD} - \text{OD})|/\text{OD} \times 100 \quad (1)$$

where DE is the dimensional error as a percentage, SD is the scanned dimension, OD is the original dimension, and $|(\text{SD} - \text{OD})|$ is the absolute difference between the SD and OD.

$$\text{VE (\%)} = |(\text{SV} - \text{OV})|/\text{OV} \times 100 \quad (2)$$

where VE is the volumetric error as a percentage, SV is the scanned volume, OV is the original volume, and $|(\text{SV} - \text{OV})|$ is the absolute difference between the SV and OV.

3. Results and Discussions

In this section, the results of the four modes of 3D scanning are presented and discussed for both samples (S1 and S2). Finally, the practical implications of all 3D scanning modes will be discussed for both S1 and S2.

3.1. Three-Dimensional Scanning of Sample 1

For mode A of 3D scanning (see Table 2) S1, the scanning factors were found to be insignificant. Almost the same percent contributions (PCRs) were demonstrated from both watertightness and simplification, as can be seen in Table 3. Of the main effects plot in Figure 5, 50% and MW were identified to be the optimal levels of simplification and watertightness as volumetric error was found to be the lowest at these levels.

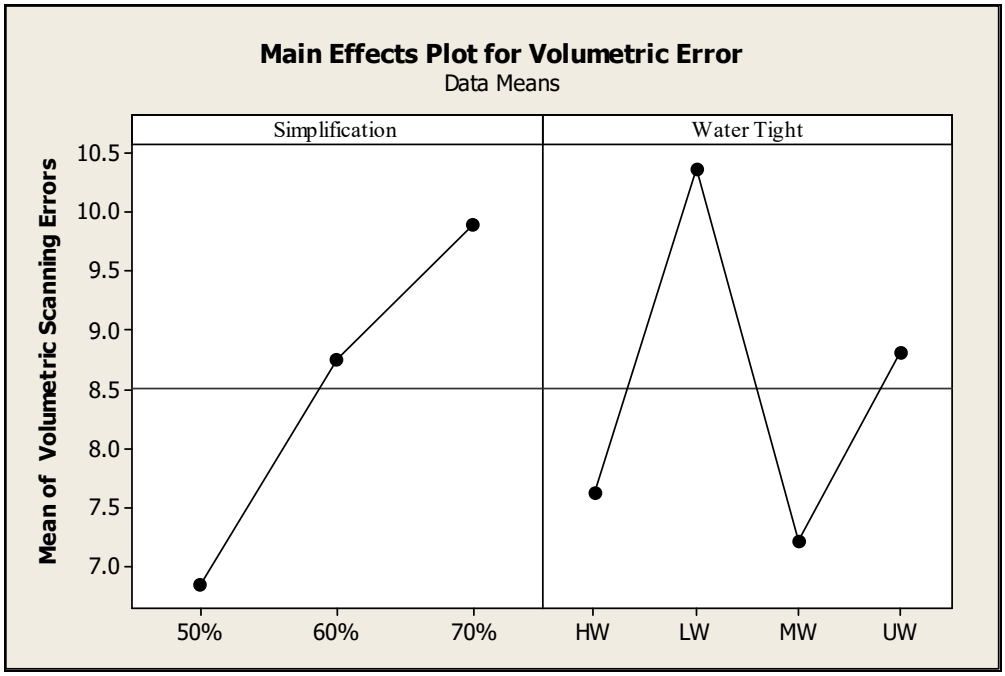

Figure 5. Main effects plot for volumetric error (Mode A).

Table 3. ANOVA for volumetric error (Mode A).

Source	DF	Adj SS	Adj MS	F-Value	*p*-Value	PCR
Simplification	2	18.87	9.43	0.5	0.64	12.30
Watertightness	3	17.94	5.98	0.3	0.82	11.69
Error	6	116.6	19.43			76.00
Total	11	153.40				

However, the error PCR was found to be the highest when compared to other PCRs for scanning factors. Therefore, a review of the interaction plots is direly needed to reveal the cause of this huge error PCR. It should be clarified here that two kinds of errors were investigated in this work. The first error investigated was the volumetric error, also called the 3D scanning error. Volumetric error may also referred to as empirical error. However, the error associated with the PCR is a statistical error that is calculated using crucial values from an ANOVA, Table 3. In an interaction plot, colorful lines usually belong to one factor, i.e., simplification in relation to another factor, i.e., watertightness, as shown in Figure 6. These lines cross each other at an angle which defines the severity index (SI) of the interaction. If the lines were parallel, the SI will be zero, representing zero interaction between the factors. Likewise, an SI of 100% implies that interaction occurs between the factors when the two lines intersect each other at a 90-degree angle. Normally, two lines intersect each other at an angular value between 0 and 90 degrees, indicating the presence or absence of interaction between the factors. If an SI value were found to be near zero percent, the interaction may be classified as a mild interaction between the factors. A severe interaction is usually present if the SI value reaches 100%. The interaction may be classified as moderate if the SI value lies between zero and one hundred percent. From the interaction plot in Figure 6, the severity index (SI) values were found to be between 70% to 89% for all possible interactions, depicting a severe degree of interaction for mode A of the 3D scanning.

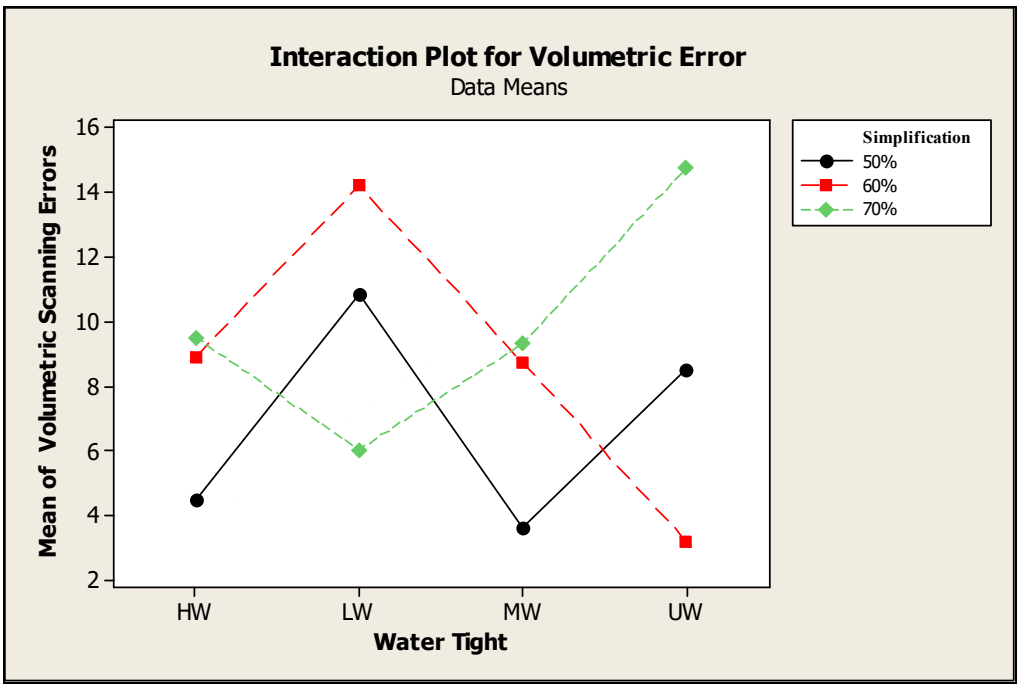

Figure 6. Interaction plots for volumetric error (Mode A).

Moreover, a severe interaction means that the levels of the two factors i.e., simplification and watertightness, do not affect the response parameter, i.e., the volumetric error in the 3D scanning independently for mode A of 3D scanning. In fact, there exists a combined

effect between the levels of simplification and watertightness that affects the quality of the 3D scanning. A high SI value is usually considered the cause of the highest error PCR and the non-significance of factors. Hence, combined effects on the 3D scanning error among the levels of watertightness and simplification cause the increased value of the error PCR.

When S1 was scanned three dimensionally with mode B, all the factors were found to be insignificant from the ANOVA for the 3D texture scan and sharpness selected in the absence of smoothness for the simple box sample, as shown in Table S1 of the Supplementary File. A MW watertightness and a simplification of 70% were the two levels of simplification and watertightness which resulted in the minimum volumetric error of the 3D scanning the simple box (i.e., S1), as can be seen from the main effects plot in Figure S2 of the Supplementary File. The PCR for simplification was found to be higher than that of the watertightness. Since the error PCR was the highest, interaction plots were made again. As the colored lines were associated with levels of simplification, they were plotted against the levels of watertightness. From Figure S3 of the Supplementary File, a maximum severity index (SI) value of 122% was achieved between 50% and 70% and between 60% and 70% for the simplification levels when the lines moved from HW and LW levels of watertightness. Likewise, when the lines of the interaction plot in Figure S3 of the Supplementary File proceeded ahead from LW to MW and from MW to UW, SIs of 111% and 105%, respectively, were achieved, indicating the same cause of a high error PCR and non-significance. Therefore, 3D scanning factors were found to be insignificant with their severe combined effects on the quality of the 3D scanning when the sharpness was ON and the smoothness was OFF.

Thus far, the texture scan was employed and the results of the 3D scan have been discussed by keeping the sharpness and smoothness alternatively ON and OFF. It can be seen in Table S2 of the Supplementary File that all 3D scanning factors were found to be insignificant when a non-texture scan was executed for Sample 1 with the smoothness ON, i.e., using mode C of 3D scanning. Of the plot of the main effects in Figure S4 of the Supplementary File, MW and a simplification of 70% were found to be the optimal levels of watertightness and simplification as crucial levels of the 3D scanning factors for minimizing the volumetric error. Moreover, the PCR of simplification was evaluated to be higher than that of the watertightness. However, the error PCR was found to be somehow lower among all the PCRs. Hence, it was again necessary to find the cause of the slightly higher error PCR by looking at the interaction plot. Though the error PCR was marginally higher when compared to the PCR of watertightness only, it was expected that a moderate level of severity of interaction was also present. After seeing the interaction plot for volumetric error from Figure S5 of the Supplementary File, a combined effect of different levels of watertightness and simplification was found with an SI of 35% between MW and UW for line abscissa of 50% and 60%, as expected. Hence, the cause of the moderate value of the error PCR was solely based on this interaction.

From Table S3 of the Supplementary File, the 3D scanning factors were found to be insignificant when the non-texture scanning mode and sharpness were ON and the smoothness was OFF (as per 3D scanning mode D of Table 2), with a PCR of watertightness that was higher than the PCR of simplification for Sample 1. A value of the error PCR lay between simplification and watertightness, implying lower and higher values than the PCRs of watertightness and simplification respectively. The error PCR was found to be slightly higher again, as was found in mode C, suggesting a close look at the interaction plots, which usually provide crucial hints toward finding the cause of a higher error PCR. Upon exploring the interaction plot, which is shown in Figure S7 of the Supplementary File, a severity index (SI) of 35.56% was found for almost all the possible interactions between the various levels of watertightness and simplification, as expected from the moderate value of the error PCR in Table S3 of the Supplementary File. This value of SI is considerable, and it indicates that combined effect of the levels of both watertightness and simplification exists with mild severity in the 3D scanning error. This also implies that the error PCR was evaluated to be slightly higher due to this combined effect. Moreover, the

main effects pointing toward optimal levels of 3D scanning factors were found to be UW and 70% for the watertightness and simplification, respectively, as shown in Figure S6 of the Supplementary File.

Practical Implications of Modes of 3D Scanning for Sample 1

The dimensional errors were calculated to be minimized by identifying the optimal combination of 3D scanning factors as per the full factorial DOE used. An analysis of variance (ANOVA) was performed to find the significance of the scanning factors for the dimensional errors at a confidence level of 95%. A 3D scanning factor was declared to be significant if its *p*-value was found to be less than 0.05. Volumetric errors were finally calculated in real and virtual ambiences using CMM and Solidworks, respectively.

Overall, regardless of their utilization before or after scanning, none of the 3D scanning factors were found to be significant for S1. These 3D scanning factors had lower PCRs for watertightness and simplification throughout when compared to the higher error PCRs for all four modes of scanning for Sample 1 except for modes C and D. In modes C and D, the error PCR was slightly lower than that of one scanning factor, which may be neglected. The interaction plots were worth plotting as the error PCRs were found to be higher and all the scanning factors were found to be insignificant since combined effects may be suspected and expected to be significant and are a reason for achieving higher values of error PCRs.

From the interactions (Figure 6 and Figures S3, S5, and S7 of the Supplementary File), our overall findings depict that the error PCRs were found to be higher than the PCRs of the 3D scanning factors for all modes of 3D scanning. This indicates that the independent effect of a 3D scanning factor on reducing 3D scanning errors is frequently absent due to greater values of SIs and the presence of interactions or the combined effects of various 3D scanning factors on the 3D scanning error. Therefore, the 3D scanning factors interact with each other, or their impact on the 3D scanning error is only possible if they act together simultaneously.

Main or independent effects were also considered to find the optimal levels of 3D scanning factors that cause minimal volumetric errors. PCRs and *p*-values, which demonstrate the significance of the 3D scanner factors, indicate the overall independent vitality or significance of a single factor without describing the significance of its levels.

As far as the plots of the main effects are concerned, a MW level of watertightness was found to be the optimal level for modes A, B, and C but not mode D, which demonstrated an optimal watertightness level of UW. Additionally, 70% was found to be the optimal level of simplification for modes B, C, and D but not mode A, which demonstrated an optimal simplification level of 50%.

Of the results, it can be deduced that the 3D scanning of simple objects may provide unnecessary errors as 3D scanning modes require either smoothness or sharpness or both to prepare the scanned models for 3D/4D printing. This may take more time when compared to the geometric modeling of simple objects. In other words, the 3D scanning of simple objects may result in handling a complex data analysis, making it more intricate in terms of time, cost, precision, and accuracy than geometric modeling. Although the significance of the 3D scanner factors is crucial for the significance of both the factors of S1 and S2 towards a simple object, they are less reliable as 3D scanners are typically used for intricate objects that do not have blueprints or drawings. This is also true because simple objects may be conveniently geometrically modeled without errors. This implies that the simple models should necessarily be digitized via Solidworks or 3D modeling software instead of conducting a 3D scan.

3.2. Three-Dimensional Scanning of Sample 2

From Table S4 of the Supplementary File, watertightness was found to be significant and simplification was again found to be insignificant for a texture scan with the smoothness ON and the sharpness OFF (as per mode A of 3D scanning, Table 2 of the main manuscript) for complex object S2. As watertightness was significant, its PCR value was the highest out of all the other factors. Moreover, a simplification of 70% and UW were found to be

the optimal levels from the main effects plot, shown in the Figure S8 of the Supplementary File, toward reducing the volumetric error after the complex object was scanned three dimensionally. However, the error PCR was still, higher than the PCR for simplification. Therefore, the interaction plots were made again to determine whether there a combined effect of both simplification and watertightness was present or not. In Figure S9 of the Supplementary File, the lines starting from HW to LW had an interaction with a severity index (SI) of 88.89% between 50% and 70% levels of simplification. Likewise, an interaction with an SI of 61.12% was found for the same levels of simplification when the lines in the interaction plot proceeded ahead from LW to MW. Therefore, these levels of simplification, i.e., 50% and 70%, affected the error in 3D scanning when they were combined with HW and LW. On the other hand, an interaction with an SI of 50% was also found between 50% and 60% when the lines of the interaction plots started at LW and ended at MW. Negligible interactions are found for the line regions between MW and UW. Therefore, severe interactions are found when the lines started from HW, and their severity reduced as they approached UW. Furthermore, the presence of severe interactions can be determined to be the real cause of a higher PCR value than that of simplification.

For S2, using the texture mode of 3D scanning with the sharpness ON and the smoothness OFF (as per mode B of 3D scanning of Table 2), all the 3D scanning factors were found to be insignificant, as is shown in Table S5 of the Supplementary File. As far as the PCRs were concerned, the watertightness PCR was evaluated to be higher than the PCR of simplification. Unfortunately, the error PCR was again evaluated to be higher than the other PCR values. Hence, it is highly likely that combined effects were present. This can be seen clearly with the help of interaction plots. A maximum SI value of 72.23% was also found for the possible interactions, as shown in Figure S11 of the Supplementary File. Furthermore, the plot of the main effects indicated that 60% and MW were the optimal levels of simplification and watertightness, respectively, as shown in Figure S10 of the Supplementary File.

From Table S6 of the Supplementary File, all 3D scanning factors were found to be insignificant when the non-texture modes of scanning and smoothness were ON and the sharpness was OFF (as per mode C of 3D scanning of Table 2) with the S2 sample. The simplification PCR was evaluated to be higher than the watertightness PCR. The error PCR was evaluated to be the highest among all PCRs. The plot of the main effects indicated that MW and 50% were found to be the optimal levels of watertightness and simplification, respectively, as shown in Figure S12 of supplementary file, toward reducing the 3D scanning error with mode C of 3D scanning. However, the highest error PCR suggested plotting the interaction plots to find its cause. From the interaction plot shown in Figure S13 of the Supplementary File, it was quite evident that the SI was found to be significant with a value greater than 75% and lower than 84% for all kinds of possible interactions between possible combinations of levels of watertightness and simplification. Hence, the error PCR was found to be the highest in Table S6 of the Supplementary File due to the higher value of SI associated with the combined effect of various levels of watertightness and simplification on reducing the 3D scanning error with mode C.

For the S2, when the non-texture mode of 3D scanning and sharpness were ON and the smoothness was OFF, as per mode D of 3D scanning of Table 2, watertightness and simplification were found to be insignificant. Moreover, the main effects indicated that MW and a simplification of 70% were found to be the optimal levels of both watertightness and simplification, respectively, as shown in Figure 7. The PCR of watertightness was found to be higher than that of simplification. Furthermore, the PCR of simplification was found to be the lowest among all the 3D scanning factors including the error PCR, which was found to be the highest of all, as shown in Table 4. Hence, a dire need existed to examine the interaction plot as the error PCR found was considerable. However, the 3D scanning factors were insignificant as well, which further implied that a critical look at the interaction plots was necessary. From the interaction plots in Figure 8, it was found that the SI values ranged between 75% and 80%; these were still considerable, implying that a combined effect of the

various of levels of watertightness and simplification existed and contributed toward the 3D scanning error with mode D.

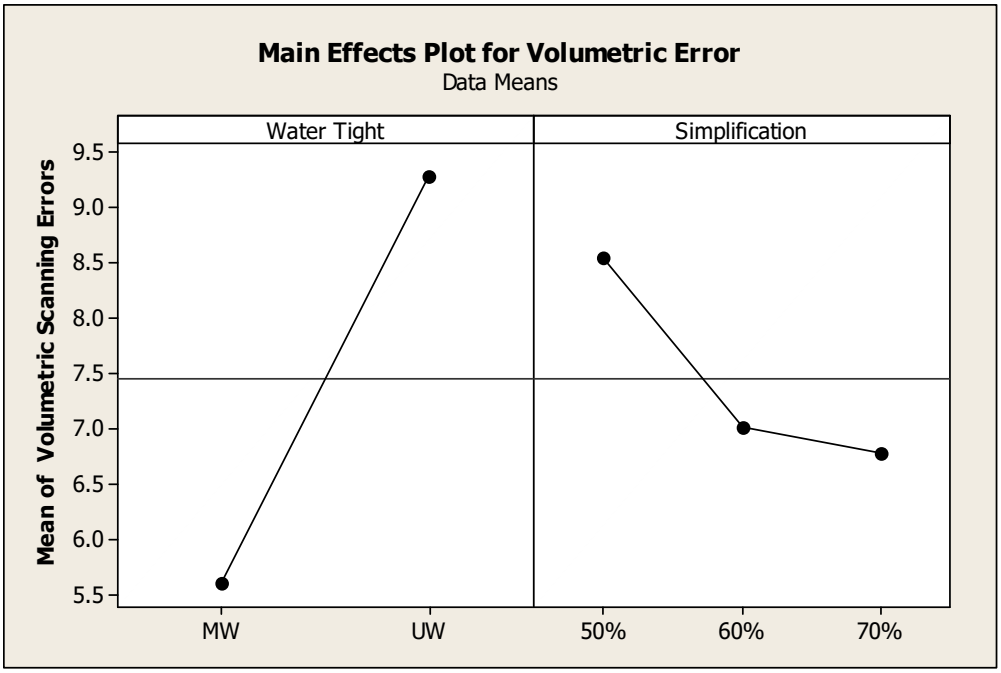

Figure 7. Main effects plot for volumetric error (mode D).

Table 4. ANOVA for volumetric error (mode D).

Source	DF	Adj SS	Adj MS	F-Value	*p*-Value	PCR
Watertightness	1	20.157	20.157	0.54	0.538	20.53
Simplification	2	3.663	1.831	0.05	0.953	3.73
Error	2	74.321	37.160			75.72
Total	5	98.141				

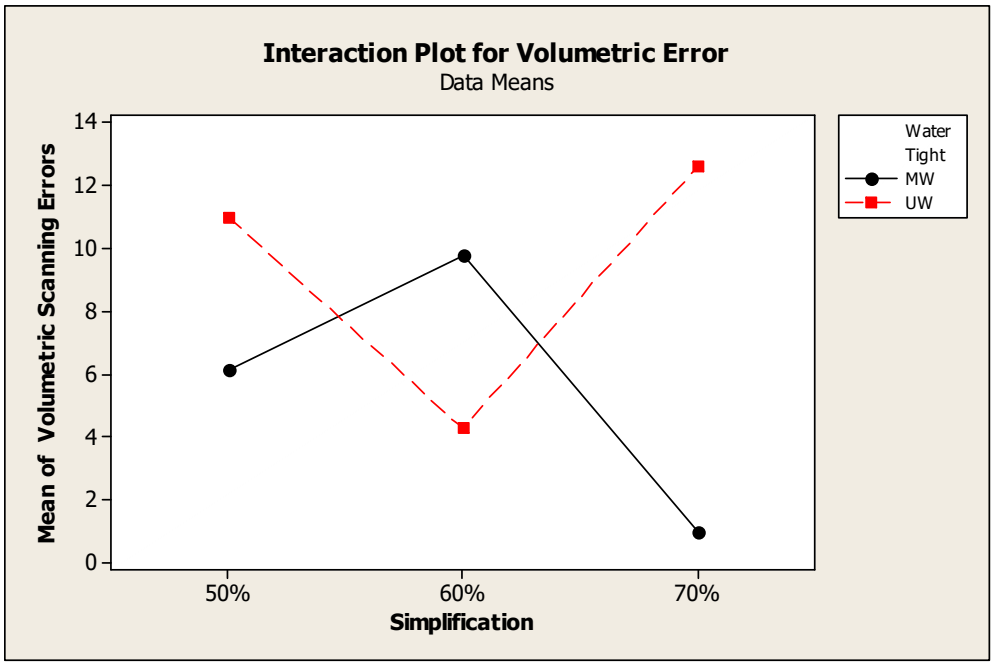

Figure 8. Interaction plots for volumetric error (mode D).

Practical Implications of Modes of 3D Scanning for Sample 2

Watertightness and simplification were the two 3D scanning factors which were essentially present in all modes of 3D scanning and were equally likely for both sample geometries. In mode A, watertightness was found to be significant toward reducing the volumetric error for Sample 2. The two 3D scanning factors, i.e., watertightness and simplification, were found to be insignificant for all modes of 3D scanning when Sample 1 was scanned. Hence, the results of 3D scanning of Sample 2 are worth investigating for their useful implications, further indicating that complex sample geometries should be scanned three dimensionally because 3D scanning them saves time and complex computational costs compared to geometric modeling. Cost and time have now become the standard and ultimate requirements in the complex global market competition among products, in making quick decisions for performing or not performing medical surgeries, and in conducting rapid reverse engineering.

From the results for S2, mode A additionally implied that 3D scanning is accomplished with both texture and smoothness. Hence, texture scans will be preferred to non-texture scans and smoothness. A likely reason for preferring the texture scan to the non-texture scan is that a detailed scan is only possible with the texture option as it has four levels of watertightness, which are reduced to two levels with a non-texture scan. Although 3D scanning is undoubtedly possible with the non-texture option, the chances of leaving out fine details of the 3D complex object during 3D scanning should be prevented from happening. Likewise, the probability of leaving crucial object details during scanning is expected to be higher when the non-texture option is used. Since both S1 and S2 were colorful in this research, the texture scan should necessarily and logically be opted for, as in mode A of 3D scanning these objects.

As far as the plots of the main effects are concerned, MW was found to be significant for modes B, C, and D but not for mode A, which demonstrated that UW was the optimal level. A level of simplification of 70% was found to be optimal for modes A and D, with simplification levels of 60% and 50% preferred for modes B and C, respectively. Additionally, when considering both Samples 1 and 2, a few common main effects and optimal levels can also be deduced, which include a simplification of 70% and MW. In other words, these two optimal levels of watertightness and simplification were frequently found to be the potential cause of a substantial reduction in errors for more than fives modes of 3D scanning regardless of sample geometry. Conclusively, watertightness with medium detail (MW) and high level of simplification, i.e., 70%, may be selected as optimal levels for all modes of 3D scanning to achieve a good dimensional agreement between the real and digital models of S1 and S2, implying a considerable reduction in 3D scanning errors. Finally, the likelihood of obtaining few errors may be further minimized with texture and smoothness. Sharpness may or may not be employed, as per the findings from results for all modes of scanning both samples. However, the selection of sharpness, in addition to optimal levels of watertightness, simplification, texture, and smoothness, can only be justified for its positive impact on 3D scanning and 3D/4D printing with the help of a macro (visual) and micro (microscopy) examination of the 3D scanned objects and 3D printed objects, respectively. In this work, the macro examination of 3D scanned objects was already performed with various modes of 3D scanning. The micro examination of the 3D printed parts will be accomplished in the future.

Of the ANVOVA tables for both samples, S1 and S2, UW was found to be an optimal level of watertightness along with a simplification of 70% simplification for only two modes of 3D scanning: mode D and mode A for Sample 1 and Sample 2, respectively. Mode D for sample 1 was not of paramount importance because it seems appropriate for Sample 1 to be modeled geometrically in 3D without being scanned. Likewise, mode D of 3D scanning for S2 also seems inappropriate due to the presence of non-texture with the additional drawback of the absence of smoothness. However, mode A of scanning Sample 2 was already recommended due to various interesting findings associated with it. For mode A, UW was found to be optimal with the texture option implying, that HW, MW, and

LW resulted in higher scanning errors when compared to the errors from setting UW. UW is a level of watertightness that requires further improvements in scanning due to its open-loop scanning outcome. Generally, open-loop scanned data are never considered ready for additive manufacturing processes, or the 3D scanned model demands further steps to improve the scanned point cloud data. Luckily, mode A already has a built-in solution to this problem as a complete package with a high level of simplification, i.e., 70%, and smoothness. Both features of mode A can sufficiently handle the further processing requirements of 3D scanned data in terms of point cloud adjustments and noise reductions in the data. Therefore, the apparent concern with UW for mode A is actually and amazingly fixed rather covered by the simultaneous presence of high simplification and smoothness for mode A. This may be considered a likely reason for the suitability of mode A for the 3D scanning of complex objects such as Sample 2. Based on the current research findings, mode A of 3D scanning should be conclusively recommended for scanning complex objects when compared to the other modes (B, C, and D) of 3D scanning. This recommendation for mode A can also be confirmed by various earlier studies [3,32] due to its capability to remove errors in the postprocessing phase of 3D scanning. Watertightness, simplification, and smoothness were already defined earlier in Section 2 as the post-scanning/post-processing 3D scanning factors with significant contributions towards mitigating possible 3D scanning errors. Therefore, the current study is in good agreement with the previous work.

Moreover, it can also be found from the ANOVA Tables for S2 that the error PCRs (i.e., the statistical error) were found to be higher for all modes of 3D scanning, i.e., B, C, and D, except for mode A with reference to Sample 2. Similarly, the error PCR was much lower than the PCR of watertightness and significantly higher than the PCR of simplification for mode A. With mode A, the simplification PCR was found to be extremely low towards reducing the 3D scanning error. Hence, the role of watertightness is crucial when adopting modes A, B, and D of scanning except for mode C, which demonstrated a higher simplification PCR was than the PCR of watertightness.

Though the error PCRs were found to be the highest in almost all the modes of 3D scanning, this directly reveals that the combined effects are likely affect the 3D scanning error positively. When considering all modes of scanning, this was not the case for S1 as error PCRs were also found to be lower for modes C and D, though the overall error PCRs in all modes of scanning for Sample 1 were found to be higher than the PCR of at least one scanning factor. Hence, a great extent of interaction between the 3D scanning factors (especially watertightness and simplification) possibly occurred to mitigate the scanning error regardless of the samples' geometry.

Apart from the statistical errors, e.g., the error PCRs, the volumetric scanning errors were found to be lower, considering the lower values of the error range for S2 compared to S1. To be terse, scanning errors for the complex sample were reduced by up to 0.1%. Such a low value of error was never before achieved; however, a dimensional error of up to 0.33% was reported in a previous study [11]. This is still higher than the dimensional error of the current research study. Upon further comparison with the literature on non-contact 3D scanners, the dimensional errors were successfully reduced by up to 3% [33], 2.5% [2], 5% [34], 6% [35], and 16% [36]. Therefore, a reduction of these errors up to 0.1%, as obtained in the current study, has never been achieved before.

Moreover, the error PCR was always found to be higher with insignificant scanning factors for mode B when considering both sample geometries as mode B involves using a texture scan with sharpness. Hence, sharpness may be treated as the secondary 3D scanning factor, even with texture option. When comparing the smoothness and sharpness, the effect of smoothness (applied together with other 3D scanning factors, as per Table 2) was found to be better than that of sharpness on mitigating the scanning errors.

As far as the PCRs of the 3D scanning factors are concerned, the watertightness PCR was generally found to be higher than that of the simplification PCR for all modes of scanning except mode C for S2. Contrarily, the simplification PCR was found to be higher than the watertightness PCR for all modes of scanning for S1 except for mode D.

Watertightness and simplification are both crucial for precise and accurate 3D scanning results for various geometries.; however, watertightness takes primary importance in 3D scanning as it can readily deliver digital models for additive manufacturing with some secondary modifications in terms of adjusting the point cloud sizing with fitting polygons, which is usually accomplished via simplification. This again validates that intricate geometries are good candidates for 3D scanning instead of simple objects, which can easily be geometrically modeled using a CAD software.

4. Conclusions

Dimensional errors were identified and reduced by considering the geometrical parameters, e.g., the lines, curves, areas, and volumes of both the real and scanned objects. The three-dimensional objects were measured physically and virtually using CMM and SolidWorks, respectively. Volumetric errors were measured by comparing the 3D scanned volume and original volume from the CMM. Three-dimensional scanning factors were optimized with full factorial DOE, comprising four novel frameworks of 3D scanning for both simple and complex objects to minimize volumetric errors. Apart from the statistical errors (e.g., error PCRs), the volumetric scanning errors were found to be lower, considering the lower value of error range for complex geometry compared to objects with simple geometry. Concisely speaking, scanning errors for the complex sample were uniquely reduced by up to 0.1%, an extent which has never before been reported by earlier studies.

The main contributions of this study are as follows:

- A simple object has complexity in scanned data for all modes of 3D scanning in terms of insignificant factors and high values of severity indices (SIs) which cause high error PCRs. Therefore, simple objects should logically and decisively be modeled using CAD software, which can save time and money instead of proceeding with 3D scanning.
- Medium detail watertightness and a simplicity of 70% were frequently concluded to be the optimal levels of watertightness and simplification in all modes of 3D scanning regardless of geometrical intricacies in simple and complex geometries.
- With mode A of 3D scanning for complex geometry, only one 3D scanning factor was significant, i.e., watertightness. However, an un-watertight watertightness and a simplification of 70% were the optimal levels of watertightness and simplification, respectively, for complex geometry. This implies that mode A is recommended for scanning complex objects which have detailed scanning specifications, e.g., texture, smoothness, and all four levels of watertightness.
- Irrespective of the sample geometry, error PCRs were lower for mode A and complex geometry. Hence, a combined effect of more than two levels of 3D scanning factors was expectedly significant in all modes of 3D scanning, helping us to justify the reason for which all modes of 3D scanning frequently delivered statistically insignificant factors except mode A for complex geometry. This is another way of verifying the suitability of mode A for the 3D scanning of complex objects.

Future studies may be aimed at reducing the 3D scanning error using mode A of 3D scanning for those physical objects which have a moderate to high level of geometrical intricacy. In other words, simple objects will be excluded in favor of the inclusion of complex objects for 3D scanning. Scanned complex objects are also deemed essential in future studies because they are ideal candidates for additive manufacturing with the additional intention of saving unnecessary cost and time and achieving more precision and accuracy in terms of their geometrical dimensions and configurations.

Supplementary Materials: The following supporting information can be downloaded at: https://www.mdpi.com/article/10.3390/app13053303/s1, Figure S1: EinScan 3D Scanner; Figure S2: Main effects plot for Volumetric Error (Mode B); Figure S3: Interaction plots for Volumetric Error (Mode B); Figure S4: Main effects plot Volumetric Error (Mode C); Figure S5: Interaction plots for Volumetric Error (Mode C); Figure S6: Main effects plot for Volumetric Error (Mode D); Figure S7:

Interaction plots for Volumetric Error (Mode D); Figure S8: Main effects plot for Volumetric Error (Mode A); Figure S9: Interaction plots for Volumetric Error (Mode A); Figure S10: Main effects plot for Volumetric Error (Mode B); Figure S11: Interaction plots for Volumetric Error (Mode B); Figure S12: Main effects plot for Volumetric Error (Mode C); Figure S13: Interaction plots for Volumetric Error (Mode C); Table S1: ANOVA for Volumetric Error (Mode B); Table S2: ANOVA for Volumetric Error (Mode C); Table S3: ANOVA for Volumetric Error (Mode D); Table S4: ANOVA for Volumetric Error (Mode A); Table S5: ANOVA for Volumetric Error (Mode B); Table S6: ANOVA for Volumetric Error (Mode C).

Author Contributions: S.F.R.: conceptualization, data analysis, resources, methodology, writing—original draft; M.A. (Muhammad Amjad): methodology, data analysis, writing, investigation; K.I.: resources, review and editing, data analysis and curation; S.A.: data curation, review and editing; and M.A. (Mali Abdollahian): methodology, data analysis, writing, and investigation. All authors have read and agreed to the published version of the manuscript.

Funding: This research received funding from King Saud University through the Researchers Supporting Project, number RSP2023R387, King Saud University, Riyadh, Saudi Arabia.

Institutional Review Board Statement: Not applicable.

Informed Consent Statement: Not applicable.

Data Availability Statement: The data related to experimental findings are reported within the paper, and can be made available from the corresponding author upon a reasonable request.

Acknowledgments: The authors extend their appreciation to King Saud University for funding this work through the Researchers Supporting Project, number RSP2023R387, King Saud University, Riyadh, Saudi Arabia.

Conflicts of Interest: The authors declare no conflict of interest.

References

1. Chadha, A.; Haq, M.U.; Raina, A.; Singh, R.; Penumarti, N.; Bishnoi, M.S. Effect of fused deposition modelling process parameters on mechanical properties of 3D printed parts. *World J. Eng.* **2019**, *16*, 550–559. [CrossRef]
2. Geng, Z.; Bidanda, B. Review of reverse engineering systems–current state of the art. *Virtual Phys. Prototyp.* **2017**, *12*, 161–172. [CrossRef]
3. Pescaru, R.; Kyratsis, P.; Oancea, G. A Case Study of Reverse Engineering Integrated in an Automated Design Process. *OP Conf. Series Mater. Sci. Eng.* **2016**, *161*, 12029. [CrossRef]
4. Tóth, T.; Živčák, J. A comparison of the outputs of 3D scanners. *Procedia Eng.* **2014**, *69*, 393–401. [CrossRef]
5. Gonzalez-perez, I.; Fuentes-aznar, A. Reverse engineering of spiral bevel gear drives reconstructed from point clouds. *Mech. Mach. Theory* **2022**, *170*, 104694. [CrossRef]
6. Haleem, A.; Javaid, M. 3D scanning applications in medical field: A literature-based review. *Clin. Epidemiol. Glob. Health* **2019**, *7*, 199–210. [CrossRef]
7. Anwer, N.; Mathieu, L. From reverse engineering to shape engineering in mechanical design. *CIRP Ann.* **2016**, *65*, 165–168. [CrossRef]
8. Qie, Y.; Bickel, S.; Wartzack, S.; Schleich, B.; Anwer, N. A function-oriented surface reconstruction framework for reverse engineering. *CIRP Ann.* **2021**, *70*, 135–138. [CrossRef]
9. Bauer, F.; Schrapp, M.; Szijarto, J. Accuracy analysis of a piece-to-piece reverse engineering workflow for a turbine foil based on multi-modal computed tomography and additive manufacturing. *Precis. Eng.* **2019**, *60*, 63–75. [CrossRef]
10. Yang, Y.; Fang, H.; Fang, Y.; Shi, S. Three-dimensional point cloud data subtle feature extraction algorithm for laser scanning measurement of large-scale irregular surface in reverse engineering. *Measurement* **2020**, *151*, 107220. [CrossRef]
11. Yanamandra, K.; Chen, G.; Xu, X.; Mac, G.; Gupta, N. Reverse engineering of additive manufactured composite part by toolpath reconstruction using imaging and machine learning. *Compos. Sci. Technol.* **2020**, *198*, 108318. [CrossRef]
12. Che, J.; Zhang, Y.; Wang, H.; Liu, Y.; Du, M.; Ma, S.; Zhao, Y.; Suo, C. A novel method for analyzing working performance of milling tools based on reverse engineering. *J. Pet. Sci. Eng.* **2020**, *197*, 107987. [CrossRef]
13. Wang, P.; Yang, J.; Hu, Y.; Huo, J.; Feng, X. Innovative design of a helmet based on reverse engineering and 3D printing. *Alex. Eng. J.* **2021**, *60*, 3445–3453. [CrossRef]
14. Liu, X.; Wei, Y.; Wu, H.; Zhang, T. Factor analysis of deformation in resistance spot welding of complex steel sheets based on reverse engineering technology and direct finite element analysis. *J. Manuf. Process.* **2020**, *57*, 72–90. [CrossRef]
15. Segreto, T.; Bottillo, A.; Teti, R.; Galantucci, L.; Lavecchia, F.; Galantucci, M.B. Non-contact Reverse Engineering Modeling for Additive Manufacturing of Down Scaled Cultural Artefacts. *Procedia CIRP* **2017**, *62*, 481–486. [CrossRef]

16. Segreto, T.; Bottillo, A.; Caggiano, A.; Martorelli, M. Integration of reverse engineering and ultrasonic non-contact testing procedures for quality assessment of CFRP aeronautical components. *Procedia CIRP* **2019**, *79*, 343–348. [CrossRef]
17. Engel, B.; Al-Maeeni, S.S.H. An integrated reverse engineering and failure analysis approach for recovery of mechanical shafts. *Procedia CIRP* **2019**, *81*, 1083–1088. [CrossRef]
18. Irzmańska, E.; Okrasa, M. Evaluation of protective footwear fit for older workers (60+): A case study using 3D scanning technique. *Int. J. Ind. Ergon.* **2018**, *67*, 27–31. [CrossRef]
19. Haleem, A.; Javaid, M. Enablers, Barriers, and Critical Success Factors for Effective Adoption of Color-Jet 3D Printing Technology. *J. Ind. Integr. Manag.* **2019**, *7*, 599–625. [CrossRef]
20. Javaid, M.; Haleem, A. Additive manufacturing applications in medical cases: A literature based review. *Alexandria J. Med.* **2018**, *54*, 411–422. [CrossRef]
21. Maloney, T.R. Experimental and archaeological testing with 3D laser scanning reveals the limits of I/TMC as a reduction index for global scraper and point studies. *J. Archaeol. Sci. Rep.* **2019**, *29*, 102068. [CrossRef]
22. Andrews, E.T.; Ashton, J.; Pearson, F.; Beattie, R.; Johnson, M.J. Handheld 3D scanning as a minimally invasive measuring technique for neonatal anthropometry. *Clin. Nutr. ESPEN* **2019**, *33*, 279–282. [CrossRef] [PubMed]
23. Piperi, E.; Bodi, I. Scanning, 3D GD & T Inspection for automotive plastic elements. In Proceedings of the 9th International Textile Conference & 3rd International Conference on Engineering and Entrepreneurship 2021, Tirana, Albania, 18–19 December 2021.
24. Bodi, I.; Piperi, E.; Kaçani, J. Design and production of footwear using CAD/CAM systems. In Proceedings of the 9th International Textile Conference & 3rd International Conference on Engineering and Entrepreneurship 2021, Tirana, Albania, 18–19 December 2021.
25. Paper, C.; Spahiu, T.; Politeknik, U.; Piperi, E.; Politeknik, U. Extracting body dimensions from 3D body scanning. In Proceedings of the 6th International Conference of Textile, Tirana, Albania, 20 November 2014; Volume 20, pp.1–11.
26. Galantucci, L.M.; Piperi, E.; Lavecchia, F.; Zhavo, A. Semi-automatic low cost 3D Laser scanning systems for reverse engineering. *Procedia CIRP* **2015**, *28*, 94–99. [CrossRef]
27. Piperi, E.; Galantucci, L.; Bodi, I. 3D Low-cost scanning systems development for mechanical parts digi-talization. In Proceedings of the 1st International Conference "Engineering and Entrepreneurship", Tirana, Albania, 8–10 December 2017; pp. 1–8.
28. Vazzana, A.; Higgins, O.A.; Oxilia, G.; Lugli, F.; Silvestrini, S.; Nava, A.; Bondioli, L.; Bortolini, E.; Di Domenico, G.; Bernardini, F.; et al. Reports High-accuracy methodology for the integrative restoration of archaeological teeth by using reverse engineering techniques and rapid prototyping. *J. Archaeol. Sci. Rep.* **2022**, *44*, 103511. [CrossRef]
29. Lazarević, D.; Nedić, B.; Jović, S.; Šarkoćević, Ž.; Blagojević, M. Optical inspection of cutting parts by 3D scanning. *Phys. A Stat. Mech. its Appl.* **2019**, *531*, 121583. [CrossRef]
30. Feng, P.; Zou, Y.; Hu, L.; Liu, T. Use of 3D laser scanning on evaluating reduction of initial geometric imperfection of steel column with pre-stressed CFRP. *Eng. Struct.* **2019**, *198*, 109527. [CrossRef]
31. Javaid, M.; Haleem, A. Current status and applications of additive manufacturing in dentistry: A literature-based review. *J. Oral Biol. Craniofacial Res.* **2019**, *9*, 179–185. [CrossRef]
32. Javaid, M.; Haleem, A.; Kumar, L. Dimensional errors during scanning of product using 3D scanner. In *Advances in Engineering Design*, 1st ed.; Springer: Singapore, 2019; pp. 727–736. [CrossRef]
33. Raja, V.; Fernandes, K.J. *Reverse Engineering: An Industrial Perspective*; Springer: London, UK, 2008; p. 242. [CrossRef]
34. Ghahremani, K.; Safa, M.; Yeung, J.; Walbridge, S.; Haas, C.; Dubois, S. Quality assurance for high-frequency mechanical impact (HFMI) treatment of welds using handheld 3D laser scanning technology. *Weld. World* **2014**, *59*, 391–400. [CrossRef]
35. Azlan, K.A.; Omar, M.; Hussin, M.; Abdullah, M.; Chinniah, E.S. Measurement Accuracy Assessment for Laser Triangulation 3D Scanning Machine. *Int. J. Recent Technol. Eng.* **2020**, *8*, 2789–2793. [CrossRef]
36. Yu, F.; Zeng, L.; Pan, D.; Sui, X.; Tang, J. Evaluating the accuracy of hand models obtained from two 3D scanning techniques. *Sci. Rep.* **2020**, *10*, 1–10. [CrossRef] [PubMed]